Laser complex amplitude measurement using transverse translation-defocus diversity phase retrieval

JIAHE MENG[1], WENBO JING[1,*], BINGKUN HUANG[1], MEIHUI LIANG[1], DONGJIE ZHAO[2], KAI YAO[2]
[1]*School of Opto-electronic Engineering, Changchun University of Science and Technology, Jilin 130022, China*
[2]*School of Electronics and Information Engineering, Changchun University of Science and Technology, Jilin 130022, China*

In this paper, to effectively constrain the phase reconstruction, we demonstrate the use of Transverse Translation-Defocus Diversity Phase Retrieval (TTDDPR)as an approach for measuring the phase of the laser. The decomposed sub apertures are used to generate adequately sampled intensity patterns, a defocus plane is introduced to increase the amount of prior information for phase reconstruction. An optimization constrained by their joint influence is then employed to retrieve the phase. The simulation validation of the method is presented to measure the laser complex amplitude and the results demonstrated the feasibility and precision of the proposed method.

(Received August 19, 2024; accepted April 15, 2025)

Keywords: Laser beam quality, Phase retrieval, Phase diversity, Inverse problems

1. Introduction

The optical quality monitoring of laser beams requires complex amplitude measurements. The laser complex amplitude comprises two components: amplitude and phase. The corresponding phase cannot be recorded by a digital camera, the loss of phase information makes the laser complex amplitude reconstruction an ill-defined problem. The majority of solutions to the phase reconstruction problem involve either transforming a well-posed problem by introducing extra information or optimizing an ill-posed problem iteratively [1].

We can induce extra information to recover the phase, such as the Shack-Hartmann wavefront sensor (SH-WFS) [2-5], Holography [0-0] and the non-interferometric Transport-of-intensity Equation (TIE) [9-12]. In contrast to the method of phase recovery requiring extra information, Phase Retrieval (PR) [13-16] offers an effective method that can recover the phase distribution just from intensity-only measurements. The PR offers advantages such as not requiring additional optics to perform the measurement and the capability to measure high-order continuous wavefront aberrations. The PR has created possibilities for emerging imaging techniques [17,18], including computational and wavefront sensing. To overcome two of the ambiguity problems commonly associated with phase retrieval: defocus and twin image, a translation diverse measurement [19-23] is added to phase retrieval, which has been shown to make the problem of image reconstruction by phase retrieval much more robust.

In this paper we aim to present an approach for laser complex amplitude measurement using the TTDDPR, which constrains the phase reconstruction to solve the ambiguity problem of phase retrieval. A transversely translated sub aperture and a defocus plane are used to record adequate intensity information. The amplitude and phase of the laser are then reconstructed using a nonlinear optimization algorithm with the information. To decrease the likelihood of getting trapped in local minima, we concurrently explore a global initial value estimation algorithm based on the modified particle swarm optimization. The method is validated by simulation, and analysis and discussion are conducted on the impact of different aperture decomposition ways on the retrieval method.

2. Method

The schematic diagram for the linear transformation of complex amplitude based on TTDDPR is presented in Fig. 1(a). The measured aperture is decomposed into several sub apertures, and the intensity information of each sub aperture is obtained after the propagation of the optical field. Subsequently, the complex amplitude is reconstructed by a PR algorithm.

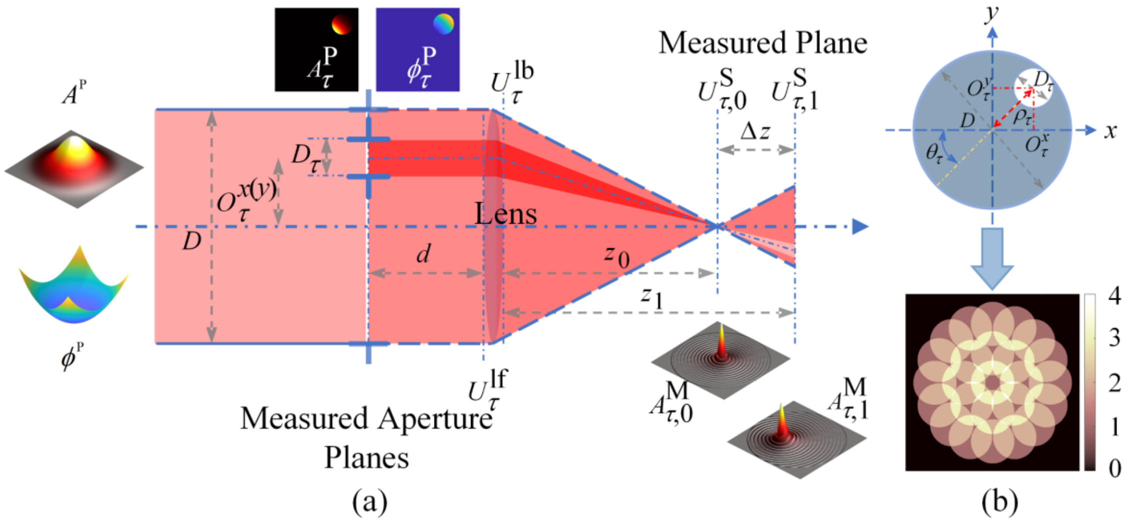

Fig. 1. Schematic diagram of TTDDPR: (a)Schematic diagram for linear transformation of complex amplitude based on TTDDPR. (b) Schematic diagram of aperture decomposition with a colour bar indicating number of sub aperture positions overlapping the pupil (colour online)

To effectively decompose the measured aperture, the aperture decomposition principle shown in Fig. 1(b) is provided to ensure that the entire measured aperture is covered by sub apertures. We reasonably select the sub aperture size based on the requirements of the optical system to minimize the negative impact of diffraction effects on information recovery. The measured aperture is divided into S radial layers, with the central sub aperture as the 0th layer. On each layer, the sub apertures are decomposed into V parts along the circumferential angle.

The index of the sub aperture τ is given by the following equation

$$\tau = \begin{cases} 0, & s = 0 \\ v + V + 2V + 3V + \ldots + (s-1)V, & s > 0 \end{cases} \tag{1}$$

where s is the index of the sub aperture layer number ($0 \le s \le S$), v is the index of the sub aperture tangential circumference ($1 \le v \le sV$). The centre offset coordinates of the sub aperture is

$$\begin{cases} O_\tau^x = \rho_\tau \cos(\theta_\tau) \\ O_\tau^y = \rho_\tau \sin(\theta_\tau) \end{cases} \tag{2}$$

where ρ_τ is the polar radius of sub aperture centre coordinates, θ_τ is the angle of the centre coordinate of the subaperture. The complex amplitude of a sub aperture can be represented as

$$U_\tau^{\mathrm{P}}(x,y) = P\left(x - O_\tau^x, y - O_\tau^y\right) A^{\mathrm{P}}(x,y) \exp\left[-j\phi^{\mathrm{P}}(x,y)\right] \tag{3}$$

The pupil function of the offset sub aperture plane is

$$P\left(x - O_\tau^x, y - O_\tau^y\right) = \begin{cases} 1, & \left(x - O_\tau^x\right)^2 + \left(y - O_\tau^y\right)^2 \le D_\tau/2 \\ 0, & \left(x - O_\tau^x\right)^2 + \left(y - O_\tau^y\right)^2 > D_\tau/2 \end{cases} \tag{4}$$

where $\left(O_\tau^x, O_\tau^y\right)$ is the centre offset coordinates of sub aperture, D_τ is the diameter of the sub aperture which cannot be longer than the measured aperture diameter D, τ is the index number of the subaperture. The distribution of the light field from the measured aperture plane to the front end of the lens U_τ^{lf}, can be expressed as

$$U_\tau^{\mathrm{lf}}(x,y) = \mathrm{OPM}\left\{U_\tau^{\mathrm{P}}(x,y), d\right\} \tag{5}$$

where $\mathrm{OPM}\left\{U_\tau^{\mathrm{P}}(x,y), d\right\}$ represents the propagation of a free space light field over a distance of d for $U_\tau^{\mathrm{P}}(x,y)$, using the Shifted Band-limited Angular Spectrum (Shifted-BLASM) method.

Neglecting the thickness of the lens, the field distribution closely fitting the back end of the lens U_τ^{lb} is

$$U_\tau^{\mathrm{lb}}(x,y) = U_\tau^{\mathrm{lf}}(x,y)\,\varepsilon_l(x,y) \tag{6}$$

where $\varepsilon_l(x,y)$ is the transmittance function of the focusing lens, f is the focal length of the lens. The distribution of the field $U_{\tau,0}^{\mathrm{S}}$ from the back end of the lens to the actual focusing plane is

$$U_{\tau,0}^{\mathrm{S}}\left(x,y\right)=\mathrm{OPM}\left\{U_{\tau}^{\mathrm{lb}}\left(x,y\right),z_0\right\} \tag{7}$$

where z_0 denotes the effective focusing axial distance of the laser through the lens. A defocusing measurement plane near the actual focusing plane is added to provide more prior information. The defocusing measurement plane field distribution $U_{\tau,1}^{\mathrm{S}}$ is

$$U_{\tau,1}^{\mathrm{S}}\left(x,y\right)=\mathrm{OPM}\left\{U_{\tau,0}^{\mathrm{S}}\left(x,y\right),\Delta z\right\} \tag{8}$$

where Δz denotes the defocused distance from the focusing plane to the defocusing plane.

Due to its simplicity and effectiveness, the mean square error is commonly used as the objective function for minimization, and it is expressed as

$$E=\sum_{\tau=0}^{\Gamma}\sum_{i=0}^{I}\sum_{(x,y)}\left|I_{\tau,i}^{\mathrm{S}}\left(x,y\right)-I_{\tau,i}^{\mathrm{M}}\left(x,y\right)\right|^2 \tag{9}$$

and

$$I\left(x,y\right)=\left|U\left(x,y\right)\right|^2=U\left(x,y\right)U^*\left(x,y\right) \tag{10}$$

where i denotes the index of the measurement plane, I ($I=1$) denotes the number of defocused measurement planes, $I_{\tau,I}^{\mathrm{M}}(x,y)$ is the measured intensity distribution in the measurement plane and $I_{\tau,I}^{\mathrm{S}}(x,y)$ is the estimation of the intensity distribution of the measurement plane.

To eliminate the influence of scaling on Eq. (9), we compared the measured intensity distribution in the measurement plane to the estimation of the intensity distribution of the measurement plane using a normalized mean square error metric

$$E=\frac{1}{\left(\Gamma+1\right)\left(I+1\right)}\sum_{\tau=0}^{\Gamma}\sum_{i=0}^{I}\frac{\sum_{(x,y)}\left|I_{\tau,i}^{\mathrm{S}}\left(x,y\right)-I_{\tau,i}^{\mathrm{M}}\left(x,y\right)\right|^2}{\sum_{(x,y)}\left|I_{\tau,i}^{\mathrm{M}}\left(x,y\right)\right|^2} \tag{11}$$

The detector on the measurement plane is easily subjected to noise during the measurement procedure, so the actual detector intensity distribution can be modelled as

$$\tilde{I}^{\mathrm{M}}\left(x,y\right)=I^{\mathrm{M}}\left(x,y\right)+n\left(x,y\right)+b \tag{12}$$

where $n(x,y)$ denotes the additive noise with a mean of zero and b denotes additive signal bias.

In order to reduce the impact of noise on the performance of the reconstruction optimization algorithm[27] and address any additional signal bias, the objective function is ultimately modified to

$$E=\frac{1}{\left(\Gamma+1\right)\left(I+1\right)}\sum_{\tau=0}^{\Gamma}\sum_{i=0}^{I}\frac{\sum_{(x,y)}w_{\tau,i}\left(x,y\right)\left|\alpha_{\tau,i}I_{\tau,i}^{\mathrm{S}}\left(x,y\right)+\beta_{\tau,i}-\tilde{I}_{\tau,i}^{\mathrm{M}}\left(x,y\right)\right|^2}{\sum_{(x,y)}w_{\tau,i}\left(x,y\right)\left|\tilde{I}_{\tau,i}^{\mathrm{M}}\left(x,y\right)\right|^2} \tag{13}$$

where $w_{\tau,i}$ are weighting terms, $\alpha_{\tau,i}$ is the signal gain factor and $\beta_{\tau,i}$ is the additive signal bias factor.

We are tasked with minimising the value of E with respect to experimental parameters. Nonlinear optimization is performed using a Limited-memory BFGS (L-BFGS) [24] optimizer for this work. To address the issue of nonlinear optimization algorithms suffering from the phase-stagnation problem with a limited initial guess, the method, named EM-PSO algorithm [25-28] for Evolutionary and Metropolis-Particle Swarm Optimization, is introduced. The EM-PSO tends to converge faster and requires fewer iterations to find a good global minimum, the EM-PSO is less likely to get stuck in local minima compared to traditional methods because it uses a population of particles to explore the search space in parallel, providing multiple opportunities to escape local traps. This makes it well-suited for the phase retrieval problem, where the initial phase is unknown and the optimization landscape is complex. The use of the EM-PSO algorithm to obtain the initial iteration value for the L-BFGS algorithm improves the convergence speed and precision of the L-BFGS algorithm.

3. Simulation and analysis

Simulation is performed to validate the effectiveness and precision of the laser complex amplitude retrieval method. The main parameters used in the simulation tests are shown in Table 1.

Table 1. The basic parameters of simulation

Parameters	Value
Wavelength (nm)	632.8
Aperture sampling diameter (pixel)	512
Image size (pixel)	1024×1024
Subapertures sampling diameter (pixel)	256
Distance between the aperture and the front end of the lens *d* (mm)	100
Aperture plane sampling spacing (μm)	5×5

37-term Zernike polynomials are used for reconstructing the wavefront, with piston set to zero. The laser complex amplitude is randomly generated as depicted in Fig. 2 (a) and (b). The measured aperture is divided into $S = 1$ and $V = 12$ as shown in Fig. 2 (c).

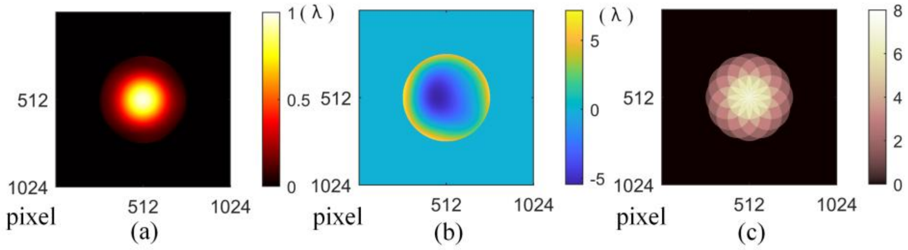

Fig. 2. Simulation data: (a) Measured amplitude. (b) Measured phase. (c) Aperture decomposition principle (colour online)

The intensity data of the focusing and defocusing measurement planes shown in Fig. 3 are generated according to the Shifted-BLASM method. The Shifted Band-limited Angular Spectrum method (Shifted-BLASM) is an improved angular spectrum propagation algorithm that enhances the accuracy and stability of wave propagation simulations. By shifting the frequency spectrum, it avoids aliasing effects and provides better performance for large-angle propagation cases. The defocused distance between the focusing measurement plane and the defocusing measurement plane is set to 15mm.

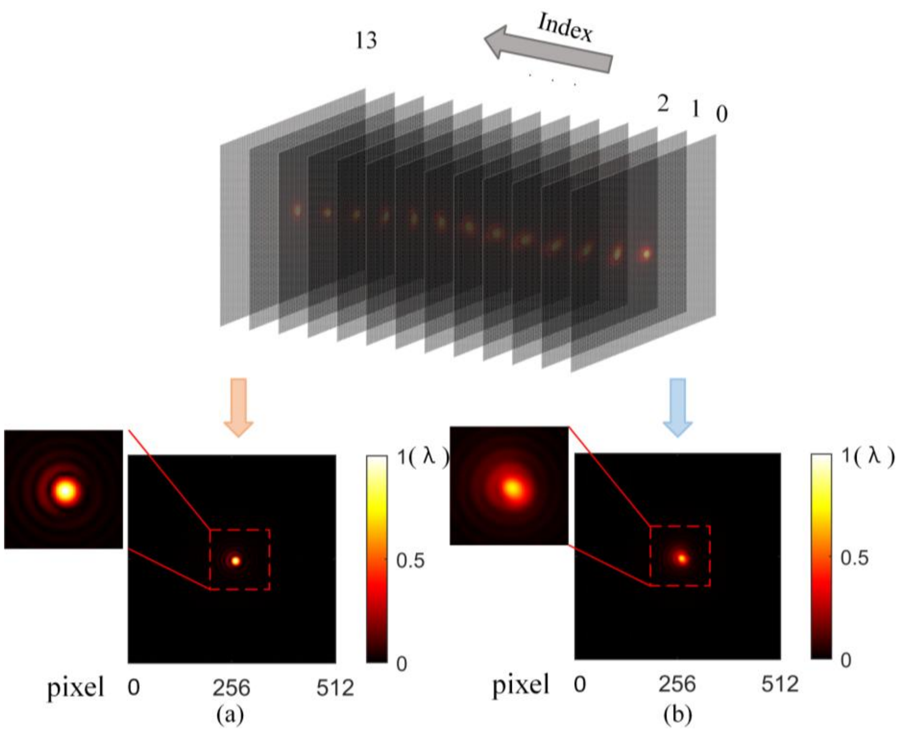

Fig. 3. Intensity images: (a) Focusing plane intensity image with index 0. (b) Defocusing plane intensity image with index 0 (colour online)

Before computing the phase retrieval error, we applied phase unwrapping to both the recovered phase and the ground truth to ensure that the error calculation is not affected by phase wrapping.

The Relative Root Mean Square Error (RRMSE) is used to measure the recovery precision of amplitude and phase in laser complex amplitude measurement.

$$\begin{cases} RRMSE_{\text{amp}} = \sqrt{\dfrac{\sum_{(x,y)} \left| A_{\text{R}}(x,y) - A_{\text{S}}(x,y) \right|^2}{\sum_{(x,y)} \left| A_{\text{S}}(x,y) \right|^2}} \\ RRMSE_{\text{pha}} = \sqrt{\dfrac{\sum_{(x,y)} \left| \phi_{\text{R}}(x,y) - \phi_{\text{S}}(x,y) \right|^2}{\sum_{(x,y)} \left| \phi_{\text{S}}(x,y) \right|^2}} \end{cases} \tag{14}$$

where $A_{\text{R}}(x,y)$ and $A_{\text{S}}(x,y)$ respectively represent the laser amplitude recovery value and the ground truth, $\phi_R(x,y)$ and $\phi_S(x,y)$ represent the laser phase recovery value and phase ground truth, respectively. The smaller the RRMSE, the higher the recovery precision. In order to analyse the relationship between the different aperture decomposition ways and the precision of laser complex amplitude reconstruction, the measured aperture is decomposed as shown in Fig. 4.

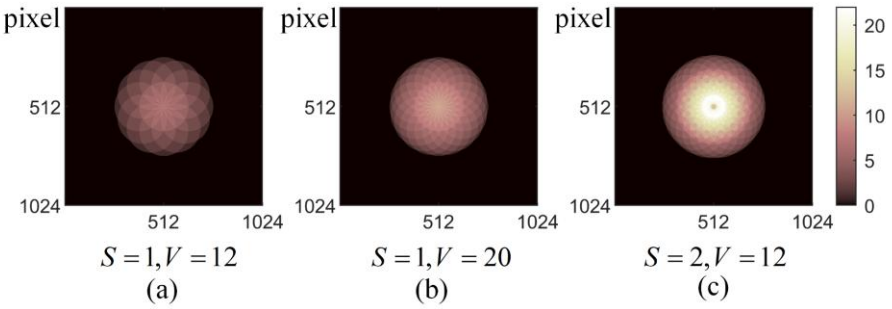

Fig. 4. Different decomposition ways of measuring aperture: (a) S = 1 and V = 12. (b) S = 1 and V = 20. (c) S = 2 and V = 12 (colour online)

Twenty sets of laser complex amplitudes are randomly generated as the ground truth. In Fig. 5, as the aperture is decomposed more finely, the precision and the stability of laser complex amplitude measurement increases. The RRMSE of amplitude and phase corresponding to S = 2 and V = 12 is 0.00037 and 0.00016, respectively. It can be seen that the precision of laser complex amplitude reconstruction based on the TTDDPR is higher, and the reconstruction stability is better than that based on the single aperture method. This could be attributed to the aperture decomposition providing more measurement data which offer additional prior information.

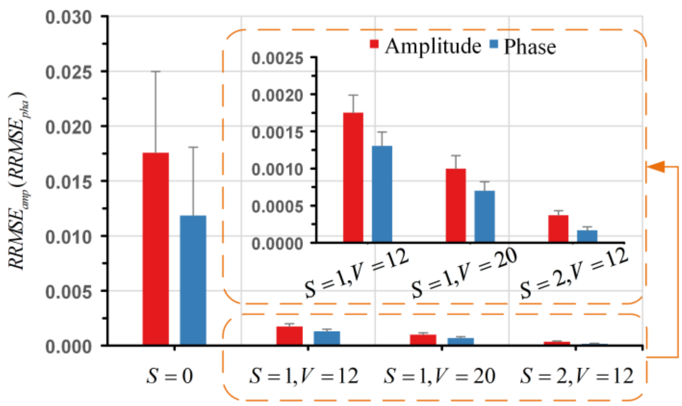

Fig. 5. RRMSE of laser complex amplitude in different aperture decomposition ways (colour online)

Fig. 6 shows the performance comparison results of PSO with different population sizes and the EM-PSO. The comparison of Zernike coefficient errors emphasizes the superior performance of the EM-PSO algorithm, particularly in achieving accurate phase initial estimations.

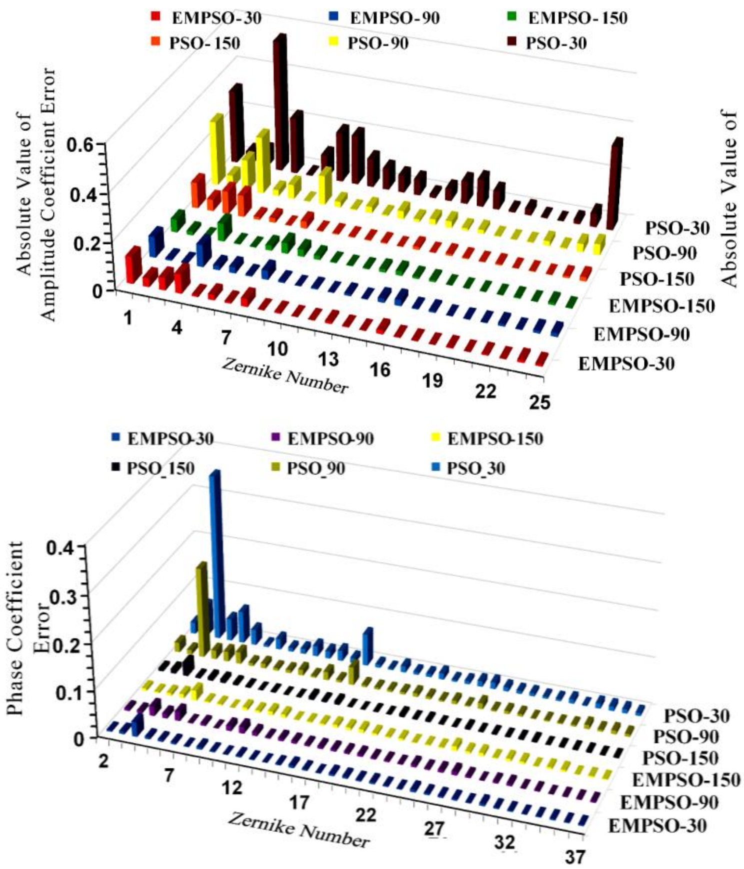

Fig. 6. Comparison of Zernike coefficient errors between PSO and EM-PSO: (a) Comparison of Zernike coefficient errors of amplitude. (b) Comparison of Zernike coefficient errors of phase (colour online)

The EM-PSO-L-BFGS algorithm is used to globally optimize the laser complex amplitude, and the result is shown in Fig. 7. It can be seen that the reconstructed amplitude and phase of laser depart very little from the ground truth. When S = 1 and V = 12, the RRMSE of the amplitude and phase between the ground truth map and the reconstructed map are 0.00125 and 0.00114, respectively, confirming the accuracy and efficiency of the method.

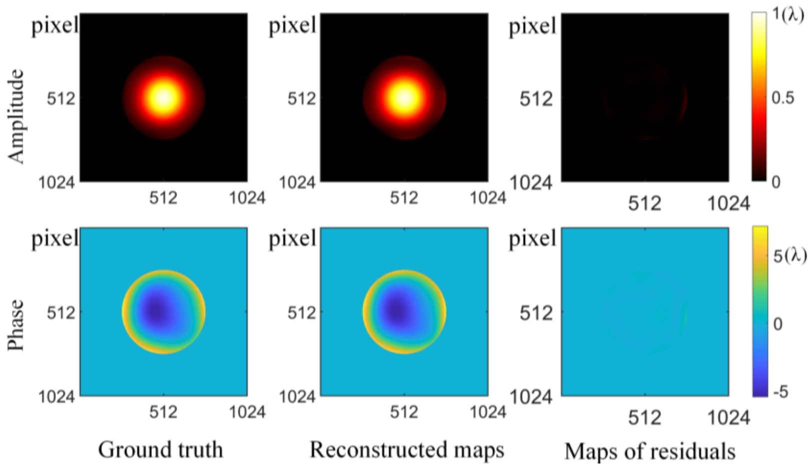

Fig. 7. Results of laser complex amplitude reconstruction (colour online)

4. Conclusion

We proposed a laser complex amplitude retrieval method using the transverse translation-defocus diversity for capturing intensity distributions from various subapertures at focusing and defocusing measurement planes. To avoid the problem of the L-BFGS algorithm getting stuck in local minima, we introduced an EM-PSO-L-BFGS algorithm. Simulation validated the effectiveness and precision of the method, demonstrating that for S = 1 and V = 12, the RRMSE for the reconstructed laser amplitude and phase can reach 0.00125 and 0.00114, respectively, validating the effectiveness and the precision of the proposed approach.

There are limitations to this simulation-based study. To further validate the effectiveness of the simulation results, the experimental verification is planned to be conducted in future work. We believe that with experimental validation, the proposed method will show great potential in practical applications.

Acknowledgements

This work is supported by the 111 project of China (D21009), Jilin Scientific and Technological Development Program (20160204009GX) and 2024 Science and Technology Research Project of Jilin Provincial Department of Education (JJKH20240922KJ).

References

[1] Kaiqiang Wang, Li Song, Chutian Wang, Zhenbo Ren, Guangyuan Zhao, Jiazhen Dou, Jianglei Di, George Barbastathis, Renjie Zhou, Jianlin Zhao, Edmund Y. Lam, Light: Science and Applications **13**, 4 (2024).
[2] R. V. Shack, J. Opt. Soc. Am. **656**, 61 (1971).
[3] Jae Jun Kim, Bautista Fernandez, Brij Agrawal, J. Opt. Soc. Am. A **38**, 456 (2021).
[4] Jia, Peng, Mingyang Ma, Cai Dongmei, Weihua Wang, Monthly Notices of the Royal Astronomical Society **503**(3), 3194 (2021).
[5] B. Pou, F. Ferreira, E. Quinones, D. Gratadour, M. Martin, Opt. Express **30**, 2991 (2022).
[6] Y. Rivenson, Y. Wu, A. Ozcan, Light Sci. Appl. **8**, 85 (2019).
[7] Yueqiang Hu, Ling Li, Yujie Wang, Min Meng, Lei Jin, Xuhao Luo, Yiqin Chen, Xin Li, Shumin Xiao, Hanbin Wang, Yi Luo, Cheng-Wei Qiu, Huigao Duan, Nano Lett. **20**(2), 994 (2019).
[8] Noah A. Rubin, Aun Zaidi, Ahmed H. Dorrah, Zhujun Shi, Federico Capasso, Science Advances **7**(33), eabg7488 (2021).
[9] Michael Reed Teague, J. Opt. Soc. Am. **73**, 1434 (1983).
[10] Chao Zuo, Jiaji Li, Jiasong Sun, Yao Fan, Jialin Zhang, Linpeng Lu, Runnan Zhang, Bowen Wang, Lei Huang, Qian Che, Optics and Lasers in Engineering **135**, 106187 (2020).
[11] Xiaofeng Wu, Ziling Wu, Sibi Chakravarthy Shanmugavel, Hang Z. Yu, Yunhui Zhu, Opt. Express **30**, 43398 (2022).
[12] Tobias Uelwer, Alexander Oberstraß, Stefan Harmeling, 25th International Conference on Pattern Recognition, Milan, Italy, IEEE, 731 (2021).
[13] D. A. Barmherzig, J. Sun, Digital Holography and Three-Dimensional Imaging, Washington, Optica Publishing Group, JTu4A-6 (2020).
[14] Yu Wu, Youming Guo, Hua Bao, Changhui Rao, Sensors **20**(17), 4877 (2020).
[15] J. R. Fienup, Appl. Opt. **21**, 2758 (1982).
[16] R. W. Gerchberg, W. O. Saxton, SPIE milestone series MS **94**, 646 (1994).
[17] Kitsada Thadson, Sarinporn Visitsattapongse, Suejit Pechprasarn. Sci. Rep. **11**, 16289 (2021).
[18] Sarinporn Visitsattapongse, Kitsada Thadson, Suejit Pechprasarn, Nuntachai Thongpance, Sensors **22**(9), 3530 (2022).
[19] Adrien Descloux, Kristin S. Grußmayer, Emrah Bostan, Tomas Lukes, Nature Photonics **12**(3), 165 (2018).
[20] Gregory R. Brady, Manuel Guizar-Sicairos, James R. Fienup, Opt. Express **17**, 624 (2009).
[21] Dustin B. Moore, James R. Fienup, Appl. Opt. **55**, 2526 (2016).
[22] Aaron M. Michalko, James R. Fienup, Opt. Lett. **43**, 1331 (2018).
[23] Nicholas J. Miller, Matthew P. Dierking, Bradley D. Duncan, Appl. Opt. **46**, 5933 (2007).
[24] D. C. Liu, J. Nocedal, Mathematical Programming **45**, 503 (1989).
[25] Nicholas Metropolis, Arianna W. Rosenbluth, Marshall N. Rosenbluth, Augusta H. Teller, Edward Teller, J. Chem. Phys. **21**, 1087 (1953).
[26] James Kennedy, Russell Eberhart. Proceedings of ICNN'95-International Conference on Neural Networks, Perth, WA, Australia, IEEE, 1942 (1995).
[27] Junhao Huang, Bing Xue, Y. Sun, Mengjie Zhang, IEEE Congress on Evolutionary Computation, Kraków, Poland, IEEE, 934 (2021).
[28] Maurice Clerc, James Kennedy, IEEE Transactions on Evolutionary Computation **20**(1), 1671 (2002).

*Corresponding author: wenbojing@cust.edu.cn